

## The Crystal Structures of One-Layer Phlogopite and Annite

ROBERT M. HAZEN, AND CHARLES W. BURNHAM

Department of Geological Sciences, Harvard University,  
Cambridge, Massachusetts 02138

### Abstract

The crystal structures of natural fluorophlogopite and annite have been refined by least-squares analysis of three-dimensional X-ray diffraction data to weighted  $R$ -values of 4.1 percent and 4.4 percent respectively. Both of these  $1M$  trioctahedral micas possess monoclinic space group symmetry  $C2/m$ . Average bond lengths for phlogopite are (Al,Si)-O 1.649, Mg-(O,F,OH) 2.064, inner K-O 2.969 and outer K-O 3.312 Å; while those of annite are (Al,Si)-O 1.659, (Fe,Mg,Ti)-(O,OH) 2.108, inner K-O 3.144 and outer K-O 3.216 Å.

Atomic fractional coordinates closely conform to the "ideal" mica structure as defined by Pabst (1955). The only significant deviations from this ideal model are tetrahedral rotation ( $\alpha$ ) and octahedral flattening ( $\psi$ ). For phlogopite  $\alpha = 7.5^\circ$  and  $\psi = 58.95^\circ$ , while for annite  $\alpha = 1.5^\circ$  and  $\psi = 58.40^\circ$ . These values agree with distortions predicted by Hazen and Wones (1972).

Anisotropies in apparent atomic vibrations may be correlated with positional disorder of aluminum and silicon in the single tetrahedral site. Magnitudes of these apparent vibrations are greater in annite, reflecting the more extensive cation substitutional disorder in that specimen.

No ordering was detected in the octahedral sheet of annite. At least 6 percent octahedral vacancies are indicated from both least-squares refinement and chemical analysis. These vacancies are evenly distributed between  $M1$  and  $M2$ , and thus do not represent solid solution between trioctahedral micas and the dioctahedral variety in which only the  $M2$  sites are occupied.

### Introduction

The first researcher to describe an X-ray diffraction examination of mica was Mauguin (1927, 1928), who determined the symmetry, unit cell dimensions, and cell content of several natural specimens. Shortly thereafter the basic crystal structure of mica was proposed almost simultaneously by Pauling (1930) and Jackson and West (1930, 1933). While several subsequent studies established the existence and geometry of complex twinning and stacking arrangements in these layer silicates (e.g., Hendricks and Jefferson, 1939; Smith and Yoder 1956; Ross, Takeda, and Wones, 1966), it was not until 1959 that a three-dimensional structure analysis of a trioctahedral mica was carried out by Takeuchi and Sadanaga (1959). A list of several recent studies on the one-layer trioctahedral mica crystal structure is given in Table 1.

Pabst (1955) presented theoretical atomic coordinates for an "ideal"  $C2/m$ , one-layer, trioctahedral mica; and this model has been subsequently described

and illustrated by several authors (e.g., Bragg *et al.* 1965, p. 254 *et seq.*). In the ideal mica structure, a sheet of regular octahedra is constrained to fit between two sheets of interconnected hexagonal rings of tetrahedra. Furthermore, basal O1 and O2 oxygens are coplanar in (001), as are apical O3 oxygen and hydroxyl groups. The above conditions imply that the interlayer cation is in the twelve-coordinated site formed by a hexagonal prism of basal oxygens. A further consequence of ideal mica geometrical constraints is the orthohexagonal unit-cell relationship,  $b = \sqrt{3} a$ .

The structure of real trioctahedral micas is most conveniently discussed in terms of deviations from the ideal model. Such deviations result from the differing sizes of ideal octahedral and tetrahedral sheets, which share the O3 oxygens. For example, it is well known that the ideal  $AlSi_3$  tetrahedral sheet of phlogopite is larger than the regular  $Mg_3$  octahedral sheet. Thus, these two sheets must coincide

TABLE. 1. Previous Studies of One-Layer Trioctahedral Mica Crystal Structures

Authors (Date)	Specimen	Refinement Conditions/Results
Takeuchi & Sadanaga (1959, 1966)	Xanthophyllite Natural	Isotropic, 3D film R = 13%
Zvyagin & Mishchenko (1962)	Phlogopite Natural	2D Electronography R = 17%
Steinfink (1962)	Ferri-Phlogopite Natural	Isotropic, 3D film R = 13%
Donnay et. al. (1964b)	Ferri-Annite Synthetic	Isotropic, 3D film R = 21%
Franzini et. al. (1963)	Six Biotites Natural	$\bar{z}$ atomic fractional coordinates from 00 $\bar{l}$ data
Takeda & Donnay (1966)	Lithium Fluor-Mica Synthetic	Anisotropic, 3D counter R = 4.8%
McCauley (1968) and McCauley et. al. (1973)	Fluor-Phlogopite Synthetic and Ba-Li-Fluor-Phlogopite Synthetic	Anisotropic, 3D counter R = 6.1% R = 7.1%
Teipkin et. al. (1969)	Iron Biotite Natural	Isotropic, 3D film R = 14%
Takeda & Burnham (1969)	Fluor-Polyolithionite Synthetic	Isotropic, 3D counter R = 5.1%

either by expansion of the octahedral sheet or by contraction of the tetrahedral sheet in the (001) plane. Radoslovich and Norrish (1962) suggest four mechanisms to accomplish this: 1) bond length alteration within the ideal sheets, 2) tetrahedral sheet tilting or corrugation, 3) octahedral sheet flattening, and 4) tetrahedral sheet rotation. Octahedral flattening and tetrahedral rotation are believed to be the most important distortions in trioctahedral micas (Donnay, Donnay, and Takeda, 1964a).

The present study is an attempt to determine the extent of deviations from Pabst's ideal mica structure for two natural specimens and to compare these deviations with values predicted by Hazen and Wones (1972). In addition, careful examinations of anisotropic atomic thermal vibration ellipsoids and octahedral occupancies and cation distributions have been made to aid our understanding of trioctahedral mica crystal chemistry.

## Experimental

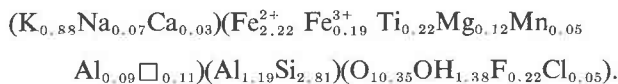
### Specimen Description—Phlogopite

Specimens of colorless euhedral phlogopite, embedded in calcite from the marbles of Franklin, New Jersey (Harvard Museum #99276), were kindly supplied by Professor Clifford Frondel. Due to the

difficulty of obtaining undeformed cleavage fragments of layer silicates, the specimen was carefully examined for single crystals of a size appropriate for X-ray diffraction studies. Eventually, a suitable euhedral hexagonal plate 60 $\mu$  thick, and 400 $\mu$  in maximum width, was selected. The structural formula of Franklin phlogopite, calculated from a wet chemical analysis (see Table 2), is  $(K_{0.77}Na_{0.16}Ba_{0.05})Mg_{3.00}Al_{1.05}Si_{2.95}O_{10.00}(F_{1.30}OH_{0.70})$ , which closely approximates the ideal phlogopite formula,  $KMg_3AlSi_3O_{10}(F,OH)_2$ . Optical properties of the crystal selected are  $\alpha = 1.530$ ,  $\beta = \gamma = 1.558$  and  $2V = 0^\circ$ . The indices of refraction are slightly higher than those of pure synthetic fluor-phlogopite ( $\gamma = 1.550$ , Hatch et al, 1957), and considerably lower than the indices of synthetic hydroxy-phlogopite ( $\gamma = 1.587$ , Hazen and Wones, 1972).

### Specimen Description—Annite

Specimens of an iron-rich, igneous biotite from the Pikes Peak Granite, Colorado, were generously provided by Dr. F. Barker of the United States Geological Survey. After optical and X-ray examination of more than thirty separated annite grains, an undeformed, approximately rectangular plate, 250 $\mu \times 400\mu \times 100\mu$  thick, was found and selected for further study. Wet chemical analysis of Pikes Peak annite was provided by Barker (Table 2). The resultant structural formula, calculated on the assumption that  $(O + OH + F + Cl) = 12$ , is



A gamma-ray resonant absorption (Mössbauer) spectrum of  $^{57}Fe$  in Pikes Peak annite was measured by Professor Roger Burns of the Massachusetts Institute of Technology, and confirmed the ratio  $Fe^{2+}:Fe^{3+} = 10:1$  in octahedral coordination. Due to the possibility of local variations in biotite composition, the single crystal under investigation was also analyzed by electron microprobe (Table 2). No zoning was observed, and the composition determined by microprobe analysis is in close agreement with wet chemical data. Optical properties of Pikes Peak annite are  $\alpha = 1.624$ ,  $\beta = \gamma = 1.672$  and  $2V = 0^\circ$ . These values are similar to those obtained by Wones (1963) for a biotite with  $Fe/(Fe + Mg) = 0.75$ .

### X-ray Diffraction

Unit cell parameters of phlogopite and annite were determined using a precision back-reflection

Weissenberg camera and measurements of both  $Cu K\alpha_1$  and  $K\alpha_2$  reflections. These data were refined using a least-squares program LCLSQ (Burnham, 1962) that corrects for systematic errors due to film shrinkage, specimen absorption, and camera eccentricity. Results of these measurements are listed in Table 3. Careful examination of  $a$ - and  $b$ -axis O-level Weissenberg photographs revealed no twinning or complex stacking arrangements. Precession photographs confirmed the diffraction symbol as  $2/mC-/-$ , resulting in  $C2$ ,  $Cm$  and  $C2/m$  as possible space groups.  $C2/m$  was selected as the trioctahedral mica space group, based on the discussion of Pabst (1955) and the experience of previous investigators (see Table 1).

Intensity measurements were made with a four-circle computer-controlled Picker diffractometer, using procedures described by Burnham *et al* (1971). All non-equivalent reflections with  $h + k = 2n$  in one hemisphere of reciprocal space within the range 0.1 to 1.0 of  $\sin \theta/\lambda$  were measured; totals were 2244 for phlogopite and 2239 for annite. Integrated intensities were corrected for Lorentz and polarization effects, and absorption corrections were computed by numerical integration (Burnham, 1966). Transmission factors varied from 0.66 to 0.92 for phlogopite, and from 0.25 to 0.62 for annite.

#### Structure Refinement—Phlogopite

All structure refinements were carried out using the full-matrix least-squares refinement program RFINE (Finger, 1969), with a weighting scheme based on counting statistics, atomic scattering factors, and rejection of unobserved reflections as described by Burnham *et al* (1971). Phlogopite refinement was initialized using the positional parameters and isotropic temperature factors of fluorophlogopite (McCauley, 1968), and, after four cycles of refinement ( $R = 8.3\%$ ), convergence was obtained. A three-dimensional Fourier difference synthesis was generated using a Fourier summation program by L. Guggenberger to detect principal sources of model error. Analysis of the Fourier map indicated that major errors were due to the presence of strongly anisotropic apparent thermal vibrations, and thus subsequent cycles of refinement included anisotropic vibration parameters. After six additional cycles ( $R = 6.6\%$ ), observations for which  $\Delta F \geq 5.0$  were rejected. 34 of 1725 observed data were rejected on this basis after convergence on the twelfth cycle ( $R = 4.1\%$ ).<sup>1</sup> A second Fourier dif-

TABLE 2. Chemical Analyses

Oxide	Franklin Phlogopite <sup>1</sup>		Pikes Peak Annite			
	Wet Analysis <sup>2</sup>		Wet Analysis <sup>2</sup>		Microprobe <sup>3</sup>	
	Wt. %	Atom # <sup>4</sup>	Wt. %	Atom # <sup>4</sup>	Wt. %	Atom # <sup>4</sup>
SiO <sub>2</sub>	42.0	2.950	33.96	2.81	33.92	2.84
$\frac{1}{2}$ Al <sub>2</sub> O <sub>3</sub>	12.7	1.050	13.10	1.19	11.87	1.16
$\Sigma$ (IV)		4.000		4.00		4.00
$\frac{1}{2}$ Al <sub>2</sub> O <sub>3</sub> (VI)		0.000		0.09		0.01
$\frac{1}{2}$ Fe <sub>2</sub> O <sub>3</sub>	0.00	0.000	3.06	0.19	36.42	0.20
FeO	0.25	0.010	32.04	2.22		2.33
MgO	28.6	2.980	0.97	0.12	0.89	0.11
MnO	0.08	0.000	0.65	0.05	0.64	0.05
NiO	0.02	0.000	0.00	0.00	--	--
ZnO	0.01	0.000	0.00	0.00	--	--
TiO <sub>2</sub>	0.22	0.008	3.55	0.22	3.61	0.23
$\Sigma$ (VI)		2.998		2.89		2.93
$\frac{1}{2}$ K <sub>2</sub> O	8.46	0.759	8.47	0.88	8.94	0.95
$\frac{1}{2}$ Na <sub>2</sub> O	1.19	0.160	0.49	0.07	0.10	0.02
$\frac{1}{2}$ Li <sub>2</sub> O	0.01	0.000	0.00	0.00	--	--
$\frac{1}{2}$ Rb <sub>2</sub> O	0.01	0.000	0.00	0.00	--	--
BaO	1.70	0.046	0.00	0.00	--	--
CaO	0.04	0.001	0.42	0.04	0.03	0.00
$\Sigma$ (alk)		0.967		1.02		0.97
$\frac{1}{2}$ H <sub>2</sub> O	1.51	0.70	2.50	1.38		1.40
F	5.85	1.30	0.82	0.22	3.35	0.22
Cl	0.00	0.00	0.34	0.05		0.05
O	--	10.00	--	10.35		10.33
$\Sigma$ (anions)		12.00		12.00		12.00
$\Sigma$ (Wt. %)	100.32		100.07		99.77	

1. Wet chemical analysis by Jun Ito, Harvard University, Cambridge, Massachusetts.
2. Wet chemical analysis by V. C. Smith, U. S. Geological Survey.
3. Microprobe analysis by Steven Roberts, Harvard University.
4. Calculated on basis of  $(O + F + Cl + OH) = 12$ , and assuming sum of tetrahedral cations equals four.

ference map was computed, on which no significant features were found.

#### Structure Refinement—Annite

Annite refinement was initialized using phlogopite atomic coordinates and isotropic temperature factors as determined above. Octahedral  $M1$  and  $M2$  sites were initially assumed to be fully occupied by  $Fe^{2+}$ , while the interlayer position was refined as 100 percent potassium. After five cycles ( $R = 12.4\%$ ) anisotropic temperature factors and real and imaginary anomalous dispersion terms (*International Tables for X-ray Crystallography*, Vol. 3, p. 215) were included. Convergence was achieved in an additional five cycles ( $R = 9.3\%$ ), and a three-dimensional difference map was generated (as described above) to determine possible sources of error. Major positive anomalies in  $\rho_{obs} - \rho_{calc}$  were detected at  $M1$  and  $M2$  octahedral sites, indicating that the 100 percent  $Fe^{2+}$  model

<sup>1</sup> Tabulated observed and calculated structure factors for phlogopite and annite are available from the authors on request.

TABLE 3. Unit-Cell Parameters of Micas Studied

Parameter	Phlogopite	Annite
$\underline{a}$ (Å)	5.3078(4)*	5.3860(9)
$\underline{b}$ (Å)	9.1901(5)	9.3241(7)
$\underline{c}$ (Å)	10.1547(8)	10.2683(9)
$\beta$ (°)	100.08(1)	100.63(1)
Vol. (Å <sup>3</sup> )	487.7(2)	506.8(2)
$\sqrt{3} \underline{a}$ (Å)	9.19	9.32
# Obs.	72	68

\* Parenthesized figures represent the estimated standard deviation (esd) in terms of least units cited for the value to the immediate left, thus 5.3078(4) indicates an esd of 0.0004.

represented too much scattering power for those sites. A moderate positive anomaly at the interlayer K position signaled the need for including a sodium contribution to that site. No other significant errors were detected.

Manganese, titanium, and iron have similar scattering factors. Thus, the contributions of these octahedral cations ( $\text{Fe}_{0.73}^{2+}\text{Fe}_{0.07}^{3+}\text{Mn}_{0.01}\text{Ti}_{0.07}$ ) in annite were conveniently modeled as  $\text{Fe}_{0.88}^{2+}$ . Similarly, aluminum and magnesium were treated as  $\text{Mg}_{0.06}$ . On the basis of wet chemical data and  $\Delta\rho_{xyz}$  magnitudes, a new composition model of ( $\text{Fe}_{0.88}^{2+}\text{Mg}_{0.06}\square_{0.06}$ ) was selected for *M1* and *M2*. The interlayer site was redefined as ( $\text{K}_{0.93}\text{Na}_{0.07}$ ), consistent with the chemical analysis. These occupancies were held constant for three refinement cycles ( $R = 5.3\%$ ), but *M1* and *M2* compositions were then allowed to vary independently, with total occupancy of each site equal to 94 percent as the only chemical constraint. After three additional cycles ( $R = 4.4\%$ ) convergence was reached with  $M1 = (\text{Fe}_{0.875}^{2+}\text{Mg}_{0.065}\square_{0.06})$  and  $M2 = (\text{Fe}_{0.883}^{2+}\text{Mg}_{0.057}\square_{0.06})$ . These values are equivalent within the estimated standard deviations ( $\pm 0.005$ ), and, thus, no preference of Fe for *M1* or *M2* was indicated.

One of the principal objectives of this investigation was to detect the existence and distribution of octahedral vacancies. In an effort to refine accurately *M1* and *M2* site occupancies, a second composition model was attempted. Octahedral cation chemistry of the Pikes Peak annite is complex, with  $\text{Fe}^{2+}$ ,  $\text{Fe}^{3+}$ , Mg, Mn, Ti, and Al in significant amounts. Furthermore, least-squares refinement procedures can permit only one occupancy variable per atom in the asymmetric unit. Thus, to refine total occupancy of the octahedral site, a suitable scattering factor model was needed to approximate the sum of scattering con-

tributions for the above elements. Since scattering power is proportional to the number of electrons,  $Z$ , a mean  $\bar{Z}$  for the octahedral sites was computed by the relation:  $\bar{Z} = \sum_i Z_i \cdot x_i$ , where  $Z_i$  is the number of electrons in the  $i$ th cation, and  $x_i$  is the fraction of that cation in the octahedral layer. The shape of scattering curves is affected by the ionic charge, and thus a mean octahedral cation charge  $\bar{C} = \sum_i C_i \cdot x_i$  was similarly calculated. Resultant values of ( $\bar{Z} = 23.2$ ,  $\bar{C} = +2.25$ ) closely approximate those of divalent manganese ( $Z = 23$ ,  $C = +2$ ). To test the validity of modelling the Pikes Peak annite octahedral sites as  $\text{Mn}^{2+}$ , the scattering curve of divalent manganese from 0.0 to 1.5  $\sin \theta/\lambda$  (*International Tables for X-ray Crystallography*, Vol. 3, pp. 202–205) was compared with a composite curve for ( $\text{Fe}_{0.73}^{2+}\text{Fe}_{0.07}^{3+}\text{Mn}_{0.01}\text{Ti}_{0.07}\text{Mg}_{0.04}\text{Al}_{0.03}$ ). Nearly perfect agreement ( $\pm 0.3$  electrons) was found for all values of  $\sin \theta/\lambda$ . Thus, *M1* and *M2* occupancies were refined using ( $\text{Mn}_{0.933}^{2+}\square_{0.065}$ ) as a composition model. After five cycles of refinement, with independent *M1* and *M2* occupancy variables, convergence was reached with  $M1 = M2 = (\text{Mn}_{0.933}^{2+}\square_{0.065})$  ( $R = 4.4\%$ ). On the final cycle, 69 of 1586 observed data were rejected with  $\Delta F \geq 5.0$ .

## Discussion

### Atomic Coordinates

The atomic coordinates and anisotropic temperature factors for phlogopite and annite are presented in Table 4 along with the "ideal" fractional coordinates of Pabst (1955) for comparison. Principal bond distances, mean coordination polyhedra bond lengths, and bond angles appear in Table 5. Refined values of atomic coordinates closely approximate those of Pabst's ideal model, and in no instance deviate more than 0.02 fractional units from them. In both structures, basal O1 and O2 oxygens are coplanar in (001), as are the apical O3 oxygen and (OH, F) positions. Note that the orthohexagonal cell parameter relationship,  $b = \sqrt{3} a$ , also applies to both specimens (see Table 3). Therefore, deviations from the ideal mica structure may be discussed solely in terms of tetrahedral rotation and octahedral flattening.

Octahedral flattening  $\psi$  is defined as the angle between a line drawn perpendicular to two parallel faces, and a line joining opposite apices of an octahedron (Donnay *et al.*, 1964a).  $\psi$  is  $54.73^\circ$  in a regular octahedron, and will exceed that value in a flattened form. In the ideal model a single value of  $\psi$  is sufficient since all octahedra are assumed to be of equal size

and shape. However, in real micas separate values of  $\psi$  may be required for the *M1* and *M2* sites. The octahedral flattening angle  $\psi$  may be easily derived from refined structural parameters as follows:

$$\cos \psi = \frac{t_o}{2 \cdot d_o},$$

where

$$t_o = 2 \left( 0.5 - \frac{2(z_{O3}) + z_{OH}}{3} \right) c \cdot \sin \beta$$

(McCauley, 1968), where  $d_o$  is the mean cation-to-anion octahedral bond distance,  $t_o$  is the octahedral sheet thickness,  $z_{O3}$  and  $z_{OH}$  are atomic fractional coordinates, and  $c$  and  $\beta$  are unit-cell parameters. For phlogopite's *M1* and *M2* octahedra,  $\psi$  angles are both  $58.96^\circ$ , while for annite they are  $58.55^\circ$  and  $58.20^\circ$  respectively. Hazen and Wones (1972) predicted values of  $\psi$  as a function of octahedral cation radius. The ionic radius of  $Mg^{2+}$  in phlogopite is  $0.72 \text{ \AA}$  (Shannon and Prewitt, 1970), while the observed cation radii of annite *M1* and *M2* are  $0.765 \text{ \AA}$  and  $0.75 \text{ \AA}$  respectively, assuming the radius of  $O^{2-}$  is the same in both annite and phlogopite. In Figure

1, plotted values of observed octahedral flattening angle  $\psi$  vs octahedral cation radius show close agreement to those predicted by Hazen and Wones (1972).

Since basal oxygens are coplanar, the tetrahedral rotation angle  $\alpha$  may be simply calculated from the  $y_{O1}$  fractional coordinate (see Fig. 2) by the relation:

$$\tan \alpha = \frac{2b(0.25 - y)}{0.50a} = 4 \frac{b}{a} (0.25 - y)$$

This may be further simplified to

$$\tan \alpha = 4\sqrt{3} (0.25 - y_{O1})$$

for those micas in which the orthohexagonal lattice relation is valid. Values of  $\alpha$  for phlogopite and annite thus calculated are  $7.5^\circ$  and  $1.5^\circ$  respectively, and agree almost precisely with magnitudes of tetrahedral rotation  $\psi$  vs mean octahedral cation radius of Hazen and Wones (1972). Predicted and refined values of  $\alpha$  as a function of cation radius are illustrated in Figure 3.

Aluminum and silicon are disordered in the tetra-

TABLE 4. Atomic Coordinates, Anisotropic Temperature Factors, and Equivalent Isotropic Temperature Factors

Atom	$x$	$y$	$z$	$\beta_{11}^a$	$\beta_{22}$	$\beta_{33}$	$\beta_{12}$	$\beta_{13}$	$\beta_{23}$	$B_{equiv}^b$
<b>Pabst (1955) Ideal Model</b>										
T	0.575	1/3	0.220							
M1	0	1/2	1/2							
M2	0	5/6	1/2							
K	0	0	0							
O1	0.305	1/4	0.160							
O2	0.055	0	0.160							
O3	0.630	1/6	0.380							
OH	0.130	0	0.380							
<b>Franklin Phlogopite</b>										
T	0.5752(1) <sup>c</sup>	0.1668(5)	0.2254(1)	0.0041(1)	0.0011(1)	0.0022(1)	-0.0001(1)	0.0004(1)	-0.00007(4)	0.57(1)
M1	0	1/2	1/2	0.0037(4)	0.0009(1)	0.0028(1)	0	0.0008(2)	0	0.61(2)
M2	0	0.8315(1)	1/2	0.0037(2)	0.0009(1)	0.0029(1)	0	0.0007(1)	0	0.62(1)
K	0	0	0	0.0205(5)	0.0066(2)	0.0071(1)	0	0.0013(2)	0	2.45(3)
O1	0.8048(3)	0.2307(2)	0.1677(2)	0.0104(4)	0.0038(2)	0.0038(2)	-0.0019(2)	0.0013(2)	-0.0002(1)	1.31(3)
O2	0.5180(4)	0	0.1675(2)	0.0149(7)	0.0026(2)	0.0028(2)	0	-0.0001(3)	0	1.25(4)
O3	0.6297(2)	0.1664(1)	0.3902(1)	0.0047(3)	0.0011(1)	0.0026(1)	-0.0000(2)	0.0008(2)	-0.0002(1)	0.64(2)
OH	0.1330(3)	0	0.4008(2)	0.0061(5)	0.0017(2)	0.0029(2)	0	0.0008(2)	0	0.80(2)
<b>Pikes Peak Annite</b>										
T	0.5703(1)	0.1665(1)	0.2246(1)	0.0075(2)	0.0024(1)	0.0036(1)	-0.0001(1)	0.0016(1)	-0.0001(1)	1.03(1)
M1	0	1/2	1/2	0.0070(3)	0.0018(1)	0.0040(1)	0	0.0022(1)	0	0.98(2)
M2	0	0.8332(1)	1/2	0.0061(2)	0.0028(1)	0.0039(1)	0	0.0014(1)	0	1.06(1)
K	0	0	0	0.0277(7)	0.0100(3)	0.0116(3)	0	0.0014(3)	0	3.65(5)
O1	0.8031(4)	0.2457(3)	0.1670(3)	0.0140(7)	0.0070(3)	0.0050(2)	-0.0028(4)	0.0025(3)	-0.0001(2)	1.98(4)
O2	0.5427(6)	0	0.1684(4)	0.0213(12)	0.0040(4)	0.0055(4)	0	0.0022(5)	0	1.96(9)
O3	0.6291(4)	0.1674(3)	0.3894(2)	0.0109(6)	0.0035(2)	0.0040(2)	-0.0004(4)	0.0017(3)	-0.0001(1)	1.34(3)
OH	0.1239(6)	0	0.3931(4)	0.0138(10)	0.0037(4)	0.0040(3)	0	0.0017(5)	0	1.48(6)

a) Equivalent isotropic temperature factors are computed according to  $B_{equiv} = 4/3 \{ \sum_i \sum_j \beta_{ij} a_i \cdot a_j \}$ , and are related in the standard way to a vibration sphere that approximates the vibration ellipsoid described by the anisotropic temperature factor tensor (Hamilton, 1959).

b) The anisotropic temperature factor form is  $\exp[-\sum_i \sum_j \beta_{ij} h_i h_j]$ .

c) Parenthesized figures represent the estimated standard deviation (esd) in terms of least units cited for the value to the immediate left, thus 0.5703(1) indicates an esd of 0.0001.

TABLE 5. Interatomic Distances and Bond Angles

Bond	Distance (Å)	Atoms	Angle (°)	Bond	Distance (Å)	Atoms	Angle (°)
<b>Phlogopite Tetrahedra</b>				<b>Annite Tetrahedra</b>			
T-01	1.648(2) <sup>1</sup>	01-T-01	108.52(6)	T-01	1.655(2)	01-T-01	108.5(1)
-01	1.651(1)	01-T-02	108.29(9)	-01	1.666(2)	01-T-02	108.7(2)
-02	1.6503(9)	01-T-02	108.50(9)	-02	1.653(2)	01-T-02	108.8(1)
-03	1.648(1)	01-T-03	110.64(7)	-03	1.661(2)	01-T-03	110.2(1)
Mean T-O	1.649	01-T-03	110.43(7)	Mean T-O	1.659	01-T-03	110.4(2)
		02-T-03	110.40(8)			02-T-03	110.4(2)
		Mean O-T-O	109.46			Mean O-T-O	109.5
01-01	2.6775(5)			01-01	2.694(5)		
01-02	2.679(2)			01-02	2.687(3)		
01-02	2.673(2)	01-01-02	59.88(7)	01-02	2.699(3)	01-01-02	59.8(1)
01-03	2.709(2)	01-01-02	60.09(6)	01-03	2.719(3)	01-01-02	60.2(1)
01-03	2.711(2)	01-01-03	60.37(4)	01-03	2.731(3)	01-01-03	60.6(1)
02-03	2.709(2)	01-01-03	60.42(4)	02-03	2.721(4)	01-01-03	60.2(1)
Mean O-O	2.693	01-02-01	60.03(0)	Mean O-O	2.702	01-02-01	60.0(1)
		01-02-03	60.38(5)			01-02-03	60.4(1)
		01-02-03	60.48(5)			01-02-03	60.4(1)
T-T [2] <sup>2</sup>	3.0634(6)	01-03-01	59.21(4)	T-T [2]	3.111(2)	01-03-01	59.3(1)
T-T	3.065(1)	01-03-02	59.12(5)	T-T	3.104(2)	01-03-02	59.2(1)
Mean T-T	3.064	01-03-02	59.27(5)	Mean T-T	3.108	01-03-02	59.3(1)
		02-01-03	60.35(6)			02-01-03	60.2(1)
		02-01-03	60.40(6)			02-01-03	60.4(1)
		Mean O-O-O	60.00			Mean O-O-O	60.0
<b>Phlogopite M1 Octahedra</b>				<b>Annite M1 Octahedra</b>			
M1-O3 [4]	2.080(1)	03-M1-O3 [2]	85.32(7)	M1-O3 [4]	2.123(2)	03-M1-O3 [2]	85.3(1)
M1-OH [2]	2.030(2)	03-M1-O3 [2]	94.68(7)	M1-OH [2]	2.119(3)	03-M1-O3 [2]	94.7(1)
Mean M1-O	2.063	03-M1-OH [4]	83.50(5)	Mean M1-O	2.121	03-M1-OH [4]	84.3(1)
		03-M1-OH [4]	96.50(5)			03-M1-OH [4]	95.7(1)
		Mean O-M1-O	90.00			Mean O-M1-O	90.0
03-03 [2]	3.067(1)	(adjacent)		03-03 [2]	2.855(5)	(adjacent)	
03-03 [2]	2.818(2)			03-03 [2]	3.121(5)		
03-OH [4]	3.067(2)	03-M1-O3 [2]	180.00	03-OH [4]	2.847(3)	03-M1-O3 [2]	180.00
03-OH [4]	2.737(2)	OH-M1-OH	180.00	03-OH [4]	3.102(2)	OH-M1-OH	180.00
Mean O-O	2.915	(opposite)		Mean O-O	2.979	(opposite)	
(adjacent)				(adjacent)			
<b>Phlogopite M2 Octahedra</b>				<b>Annite M2 Octahedra</b>			
M2-O3 [2]	2.071(1)	03-M2-O3	85.78(8)	M2-O3 [2]	2.109(2)	03-M2-O3	85.9(1)
M2-O3 [2]	2.033(1)	03-M2-O3 [2]	85.61(5)	M2-O3 [2]	2.112(2)	03-M2-O3 [2]	85.2(1)
M2-OH [2]	2.039(1)	03-M2-O3 [2]	95.18(5)	M2-OH [2]	2.083(2)	03-M2-O3 [2]	94.6(2)
Mean M2-O	2.064	03-M2-OH [2]	96.55(5)	Mean M2-O	2.101	03-M2-OH [2]	95.4(1)
		03-M2-OH [2]	83.20(6)			03-M2-OH [2]	85.6(1)
		03-M2-OH [2]	95.99(8)			03-M2-OH [2]	94.7(1)
03-03 [2]	2.818(2)	OH-M2-OH	81.18(1)	03-03 [2]	2.855(5)	OH-M2-OH	83.4(1)
03-03 [2]	2.822(2)			03-03 [2]	2.877(4)		
03-03 [2]	3.059(2)	Mean O-M2-O	90.00	03-03 [2]	3.103(2)	Mean O-M2-O	90.0
03-OH [2]	2.737(2)	(adjacent)		03-OH [2]	2.847(3)	(adjacent)	
03-OH [2]	3.063(2)			03-OH [2]	3.082(3)		
03-OH [2]	3.068(1)	03-M2-O3	178.94(9)	03-OH [2]	3.145(3)	03-M2-O3	179.7(1)
OH-OH	2.654(3)	03-M2-OH [2]	177.03(6)	OH-OH [2]	2.772(7)	03-M2-OH [2]	179.8(1)
Mean O-O	2.916	Mean O-M2-O	177.68	Mean O-O	2.976	Mean O-M2-O	179.25
(adjacent)		(opposite)		(adjacent)		(opposite)	
<b>Phlogopite Interlayer Site</b>				<b>Annite Interlayer Site</b>			
K-01 [4]	2.969(1)			K-01 [4]	3.162(3)		
K-02 [2]	2.969(2)			K-02 [2]	3.110(4)		
Mean K-O	2.969			Mean K-O	3.144		
(inner)				(inner)			
K-01 [4]	3.312(2)			K-01 [4]	3.194(3)		
K-02 [2]	3.311(2)			K-02 [2]	3.260(3)		
Mean K-O	3.3115			Mean K-O	3.216		
(outer)				(outer)			
Δ (K-O)	0.343			Δ (K-O)	0.071		

1. Parenthesized figures represent the estimated standard deviation (esd) in terms of least units cited for the value to the immediate left, thus 1.648(2) indicates an esd of 0.002.

2. Bracketed figures represent multiplicity of the bond or angle to the immediate left.

hedral sheet of a one-layer  $C2/m$  trioctahedral mica, and, thus, there is only one crystallographically distinct tetrahedral site. Consequently, the tetrahedral site composition of such a mica varies directly with the aluminum-to-silicon ratio. Smith and Bailey

(1963) noted that mean tetrahedral bond length is a sensitive function of Al/Si ratio, due to the differing sizes of these cations. Similarly, in this study, the mean  $T-O = 1.659$  Å of  $(Al_{1.21}Si_{2.79})$  in annite is greater than that of 1.649 Å for  $(Al_{1.05}Si_{2.95})$  in

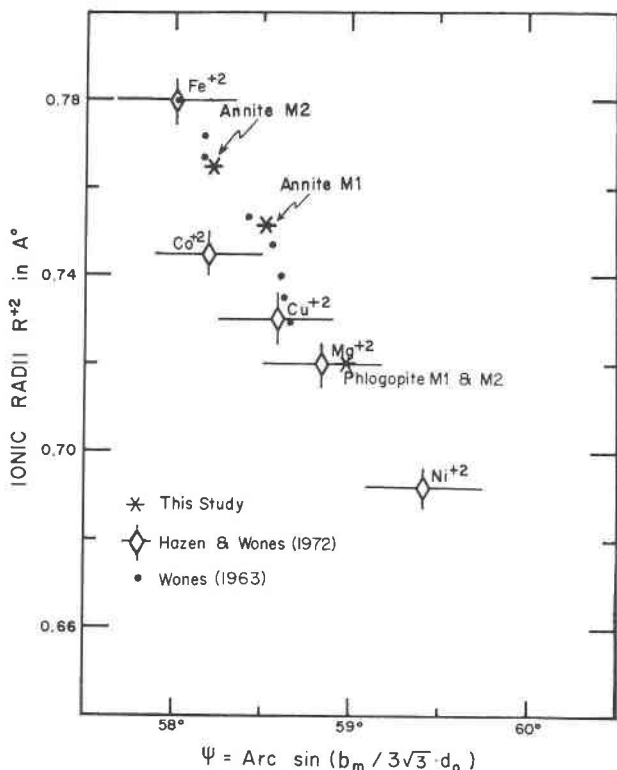


FIG. 1. Octahedral flattening angle  $\psi$  vs ionic radius of the octahedral cation for trioctahedral micas of the form  $KR_3^{+2}AlSi_3O_{10}(OH)_2$ . Black dots represent predicted values of octahedral flattening for synthetic biotites on the join phlogopite-annite by Wones (1963), while diamonds are predicted values for synthetic micas by Hazen and Wones (1972).

phlogopite. Figure 4 illustrates mean tetrahedral bond length as a function of  $x_{Al}/(x_{Al} + x_{Si})$  for several published mica structures. Linear regression analysis of this data yielded a best-fitting line of:

$$\langle T - O \rangle = 0.163 \left( \frac{x_{Al}}{x_{Al} + x_{Si}} \right) + 1.608 \text{ \AA}$$

Both annite and phlogopite tetrahedra are remarkably regular, with bond distances deviating by less than 0.5 percent of the mean, and O-T-O bond angles varying less than 1.25° from the ideal value of 109.47°.

M1 and M2 octahedral positions are crystallographically distinct and differ in nearest neighbor arrangements of oxygens and hydroxyls (or fluorines). M1 is located at a center of symmetry, with two coordinating hydroxyls at opposite apices of the octahedron, and four coordinating O3 oxygens. M2 on the other hand, is non-centric, with two adjacent

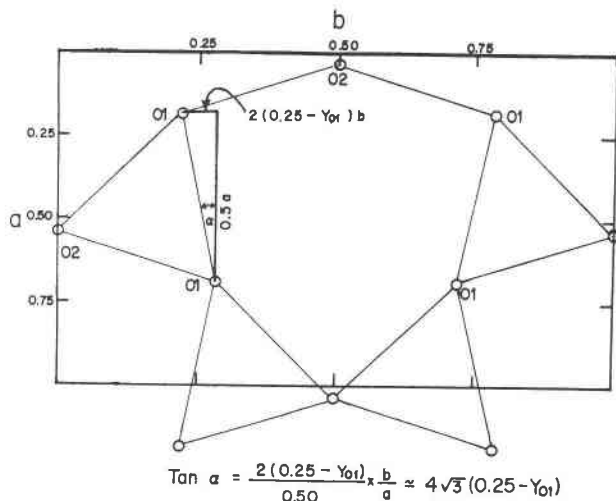


FIG. 2. Calculation of the tetrahedral rotation angle  $\alpha$  from the y fractional coordinate of atom O1. It is assumed that O1 and O2 (the basal oxygens) are coplanar. In the ideal structure (Pabst, 1955)  $y_{O1} = 0.25$ , and tetrahedral rotation is thus zero.

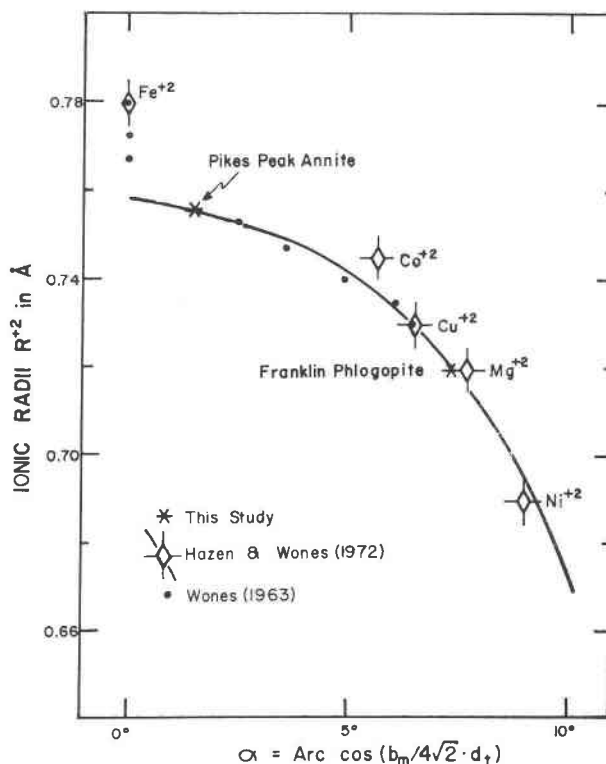


FIG. 3. Tetrahedral rotation angle  $\alpha$  vs ionic radius of the octahedral cation for trioctahedral micas of the form  $KR_3^{+2}AlSi_3O_{10}(OH)_2$ . Black dots represent predicted values of tetrahedral rotation for synthetic biotites on the join phlogopite-annite by Wones (1963), while diamonds are predicted values for synthetic micas by Hazen and Wones (1972).

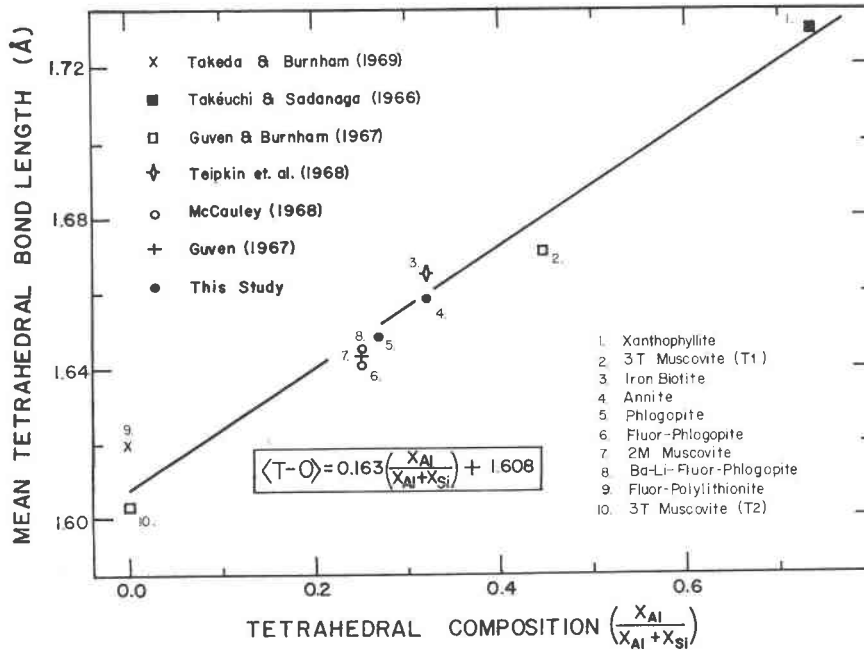


FIG. 4. Tetrahedral composition vs mean tetrahedral bond distance for micas. Regression analysis of data from this and other studies yielded a best-fitting line of

$$\langle T-O \rangle = 0.163 \left( \frac{x_{Al}}{x_{Al} + x_{Si}} \right) + 1.608.$$

coordinating hydroxyls. There are two  $M2$  octahedra for each  $M1$  in the trioctahedral layer. As previously described, octahedra are distorted through flattening in the  $c^*$  direction. Mean (OH, F)– $M$  bond lengths average 0.04 Å less than  $O3$ – $M$  bond distances, thus introducing additional octahedral distortions. Mean bond lengths of phlogopite,  $M1$ – $O$  and  $M2$ – $O$  (both 2.063 Å), are shorter than those of annite,  $M1$ – $O$  (2.122 Å) and  $M2$ – $O$  (2.102 Å).

The coordination polyhedron of the interlayer cation is sensitive to deviations from the ideal mica structure. In the ideal model, potassium is twelve-coordinated in a regular hexagonal prism. However, as ditrigonal distortion (*i.e.*, tetrahedral rotation) of the tetrahedral sheet increases, six of these coordinating oxygens move closer to, and six farther away from, the potassium. Thus with increasing rotation angle  $\alpha$ , potassium approaches six coordination in an octahedron. In annite, potassium is in nearly perfect twelve-coordination, with K–O distances ranging from 3.11 to 3.26 Å. However, in phlogopite six “inner” K–O bonds are 2.97 Å, while the other six “outer” K–O bonds are 3.31 Å in length, and potassium may be considered to be in approximately six-coordination.

In terms of octahedral flattening, tetrahedral rotation, and interlayer cation coordination, phlogopite displays significantly greater deviations from the ideal model than does annite. This implies that the misfit of ideal tetrahedral and octahedral sheets is substantially less in annite, due to its larger mean octahedral cation radius. Furthermore, Pikes Peak annite is extremely close to the ideal structure, with a tetrahedral rotation of only 1.5°. Thus, micas with an  $AlSi_3$  tetrahedral sheet are not expected to be stable if the octahedral mean cation radius is significantly larger than that of this annite, *i.e.*, 0.755 Å. This is consistent with the prediction that end-member manganous phlogopite  $KMn^{2+}_3AlSi_3O_{10}(OH)_2$  is not a stable phase (Hazen and Wones, 1972).

#### Apparent Thermal Vibrations

Magnitudes and orientations of apparent atomic vibration ellipsoids are presented in Table 6, and are illustrated in Figure 5. These apparent thermal motions are striking in both their size and anisotropies, when compared with those of other silicate minerals (Burnham, 1965). Of eight atoms in the trioctahedral mica asymmetric unit, six (*i.e.*, T, K,  $M1$ ,  $M2$ ,  $O3$ , and OH) have *rms* displacements

TABLE 6. Magnitudes and Orientation of Thermal Ellipsoids

Atom	Axis	PHLOGOPITE				ANNITE			
		rms (Å) Displacement	Angle with respect to: a (°)	b (°)	c (°)	rms (Å) Displacement	Angle with respect to: a (°)	b (°)	c (°)
T	r <sub>1</sub>	0.069(1) <sup>1</sup>	79(12)	12(12)	88(2)	0.100(2)	175(5)	89(31)	74(2)
	r <sub>2</sub>	0.075(1)	169(9)	78(12)	93(2)	0.103(2)	91(31)	177(7)	93(9)
	r <sub>3</sub>	0.107(1)	100(1)	89(2)	3(2)	0.137(1)	85(2)	93(3)	16(2)
M1	r <sub>1</sub>	0.062(4)	90	0	90	0.089(2)	90	0	90
	r <sub>2</sub>	0.071(3)	177(3)	90	83(3)	0.092(2)	10(1)	90	110(1)
	r <sub>3</sub>	0.120(2)	93(3)	90	7(3)	0.145(2)	80(1)	90	20(1)
M2	r <sub>1</sub>	0.062(3)	90	0	90	0.091(1)	0(1)	90	101(1)
	r <sub>2</sub>	0.071(2)	175(2)	90	85(2)	0.111(1)	90	0	90
	r <sub>3</sub>	0.122(2)	95(2)	90	5(2)	0.141(1)	90(1)	90	11(1)
K	r <sub>1</sub>	0.167(2)	20(4)	90	80(4)	0.179(3)	15(2)	90	85(2)
	r <sub>2</sub>	0.168(2)	90	0	90	0.210(3)	90	0	90
	r <sub>3</sub>	0.192(2)	110(3)	90	10(3)	0.248(3)	105(2)	90	5(2)
O1	r <sub>1</sub>	0.102(3)	40(3)	50(3)	94(3)	0.122(4)	153(3)	114(3)	69(4)
	r <sub>2</sub>	0.138(3)	65(13)	115(17)	149(23)	0.161(4)	99(6)	98(7)	159(4)
	r <sub>3</sub>	0.142(3)	61(12)	130(13)	60(23)	0.185(4)	64(3)	154(3)	92(8)
O2	r <sub>1</sub>	0.106(4)	90	0	90	0.132(6)	90	0	90
	r <sub>2</sub>	0.116(4)	108(5)	90	152(5)	0.167(5)	70(35)	90	171(35)
	r <sub>3</sub>	0.150(4)	162(5)	90	62(5)	0.174(5)	20(35)	90	81(35)
O3	r <sub>1</sub>	0.070(3)	94(15)	8(7)	83(3)	0.120(4)	143(25)	127(25)	79(10)
	r <sub>2</sub>	0.080(3)	176(13)	93(15)	82(4)	0.126(4)	54(25)	142(26)	106(12)
	r <sub>3</sub>	0.116(2)	92(3)	97(3)	11(3)	0.144(3)	82(7)	96(11)	20(8)
OH	r <sub>1</sub>	0.085(4)	90	0	90	0.128(6)	90	0	90
	r <sub>2</sub>	0.092(4)	175(6)	90	85(6)	0.138(6)	21(39)	90	121(39)
	r <sub>3</sub>	0.120(3)	95(6)	90	5(6)	0.145(5)	69(39)	90	32(39)

1. Parenthesized figures represent the estimated standard deviation (esd) in terms of least units cited for the value to the immediate left, thus 0.069(1) indicates an esd of 0.001.

elongated by as much as 2:1:1 approximately parallel to  $c^*$  in both phlogopite and annite. The basal O1 and O2 oxygens are less elongate than the other atoms, but the magnitudes of their equivalent<sup>2</sup> isotropic temperature factors average 85 percent greater than the apical O3 oxygens. It is improbable that such strong apparently anisotropic vibrations are due entirely to thermal motion (Burnham, 1965).

Observed anisotropic vibration ellipsoids may be correlated with positional disorder of the tetrahedral site. As previously discussed, aluminum and silicon are disordered in the single tetrahedral position. Since aluminum-to-oxygen tetrahedral bond lengths ( $\approx 1.77$  Å, from Figure 4) are considerably larger than those of four-coordinated silicon ( $\approx 1.61$  Å), oxygen positions will vary locally depending on the coordinating tetrahedral cation. Apical O3 oxygens are coordinated to one tetrahedron (see Figure 6), and, thus, the apparent thermal ellipsoids for O3 show strong elongation parallel to the bond (*i.e.*, parallel to  $c^*$ ). Basal O1 and O2 oxygens are coordinated to two tetrahedra each, thus explaining the significantly greater apparent vibrations of basal *vs* apical anions. The positions of M1, M2, K, and (OH, F) respond to local variations in oxygen positions, and large apparent vibrations are therefore

imposed on all atoms of the trioctahedral mica asymmetric unit.

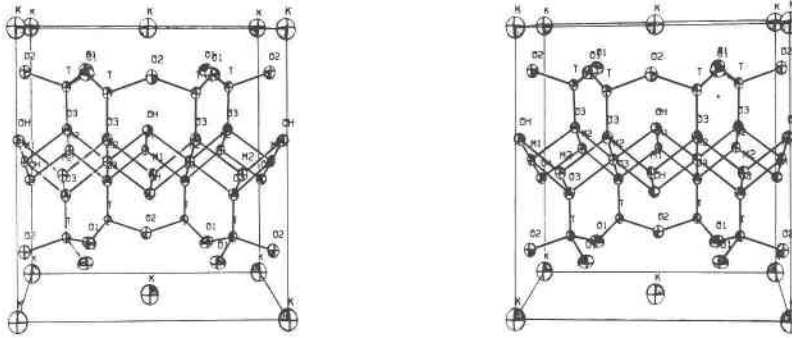
An alternative explanation of observed thermal ellipsoid elongation along  $c^*$  has been suggested by David R. Wones of the United States Geological Survey. Wones (personal communication) noted that "if F and OH are ordered in the sense that all F is in a single layer and these are randomly mixed with OH layers, then (one might observe) elongate temperature factors along  $c^*$ ." Similar arguments might be extended to ordering of cations between the mica layers.

The magnitudes of apparent vibrations in annite, as indicated by equivalent isotropic temperature factors, average 75 percent greater than those of phlogopite. This may be due to the considerable substitutional disorder in all of annite's cation sites. Not only is the content of tetrahedral aluminum greater in annite ( $Al_{1.27}Si_{2.79}$ ) than in phlogopite ( $Al_{1.05}Si_{2.95}$ ), but the octahedral and interlayer sites have complex cation occupancies as well. Thus, ellipsoids representing averaged atom positions are expected to be larger for annite than for phlogopite.

#### Annite Octahedral Site Occupancy

Refinement of octahedral occupancies using the model  $M1 = [Fe_{(0.94-x)}^{2+}Mg_x]_{0.06}$  and  $M2 = [Fe_{(0.94-y)}^{2+}Mg_y]_{0.06}$  resulted in  $x = y$  within the

<sup>2</sup> See first footnote to Table 4.



### PIKES PEAK ANNITE

FIG. 5. Stereoscopic view of one unit cell of Pikes Peak annite, showing apparent thermal vibration ellipsoids. The structure is projected with the *b*-axis vertical, the *c*-axis vertical, and the *a*-axis normal to the page. Note the elongation of ellipsoids parallel to *c*.

estimated standard deviation. However, the mean *M1*-O bond distance (2.122Å) is slightly larger than that of *M2*-O (2.102Å). Thus, while there appears to be no evidence for significant ordering of Mg and Fe in the Pikes Peak annite, ordering of Fe, Ti, and Mn may occur. It should be emphasized that the least-squares refinement program *RFINE* allows only one occupancy variable per atom in the asymmetric unit.  $\text{Fe}^{2+}$ ,  $\text{Fe}^{3+}$ ,  $\text{Mn}^{2+}$ , and  $\text{Ti}^{4+}$  possess similar scattering factor curves, and were thus conveniently modeled as  $\text{Fe}^{2+}$  in the above occupancy refinement. However, these four cations have widely differing ionic radii ( $\text{Fe}^{2+} = 0.78 \text{ \AA}$ ,  $\text{Fe}^{3+} = 0.49 \text{ \AA}$ ,  $\text{Mn}^{2+} = 0.83 \text{ \AA}$ , and  $\text{Ti}^{4+} = 0.61 \text{ \AA}$ ; Shannon and Prewitt, 1969, 1970). Thus, iron, manganese, and titanium ordering may occur, and could account for the small differences in *M1* and *M2* octahedral bond distances.

Refined values of octahedral occupancies indicate approximately 7 percent vacancies in both *M1* and *M2* sites of this annite. Other authors have suggested that as many as 15 percent of the octahedral sites are vacant in some biotites, based on calculations of structural formulae from chemical analyses (*e.g.*,

Foster, 1960). These vacancies have been assumed by several writers to represent solid solution between trioctahedral micas and the dioctahedral variety in which only *M2* positions are occupied. Such a model, however, is not valid for the Pikes Peak specimen in which equal fractions of both *M1* and *M2* are vacant.

Professor J. B. Thompson has proposed an alternative solid-solution model in which:  $\text{Ti}^{4+} + \square \rightleftharpoons 2(\text{Fe}^{2+}, \text{Mg}^{2+})$ . The resultant end-member trioctahedral micas would be:



However, since  $\text{K}(\text{FeTi})(\text{AlSi}_3)\text{O}_{10}(\text{OH})_2$  is known to be a dioctahedral mica (Wones, personal communication), it is doubtful that complete solid-solution between these end-members is achieved. Note that in this model, the atomic fraction of titanium equals the fraction of vacancies. In the Pikes Peak specimen studied,  $\text{Ti} \approx \square \approx 0.2$ , and similar results are obtained for other titanium-biotites from the Pikes Peak batholith (Barker *et al.*, 1972). Our experimental results, therefore, strongly sug-



### ANNITE TETRAHEDRA

FIG. 6. Stereoscopic view of a portion of the annite tetrahedral layer, showing apparent thermal vibration ellipsoids. Orientation is as described in Figure 5.

gest that the presence of octahedral vacancies in many natural biotites does not necessarily imply solid-solution between trioctahedral and dioctahedral end-member micas.

It is interesting to speculate on the effects of  $Ti^{4+}$  and vacancies on local charge balance in trioctahedral micas. Each apical O3 oxygen is coordinated to one tetrahedron and three octahedra. Assuming that no O3 oxygen is coordinated to more than one  $Ti^{4+}$  or vacancy, there are eight possible arrangements and electrostatic charges for the cations surrounding this oxygen:

Neighbors to O3	Charge	Neighbors to O3	Charge
(Fe + Fe + Fe) + Si	2	(Fe + Fe + Fe) + Al	1-3/4
(Ti + Fe + Fe) + Si	2-1/3	(Ti + Fe + Fe) + Al	2-1/12
(Ti + Fe + □) + Si	2	(Ti + Fe + □) + Al	1-3/4
(Fe + Fe + □) + Si	1-2/3	(Fe + Fe + □) + Al	1-5/12

Of these eight cation configurations, only three [( $Fe_3Si$ ), ( $TiFe_2Al$ ), and ( $TiFe□Si$ )] are close to the ideal net charge contribution of 2+ for oxygen. Oxygens associated with ( $Fe_2□Si$ ) and ( $Fe_2□Al$ ) are significantly undersaturated, and vacancies in such configurations would cause significant negative charge imbalances. Shortrange ordering associating titanium with vacancies could minimize this unstable local charge imbalance.

### Conclusion

Trioctahedral mica crystal chemistry is considerably simplified by the observed geometrical constraints of the layer structure. All atoms lie in one of five crystallographically distinct parallel planes (*i.e.*, K, O1-O2, T, O3-OH, and M1-M2). Thus, the mica structure may be thought of as a stacking of alternating sheets of close-packed oxygen anions and metal cations. Furthermore, the observed orthohexagonal unit-cell relation restricts the arrangements of atoms within these sheets. As a consequence, mica crystal structure discussion may be conveniently reduced to a study of two-dimensional geometry.

The structures of phlogopite and annite have been presented, in part, in the traditional terms of cation coordination polyhedra. However, an attempt has also been made to view these structures in terms of geometrical relations *within* and *between* sheets of atoms. Tetrahedral rotation is the adjustment of anions within the basal oxygen sheet, while octahedral flattening represents adjustments of spacing between sheets, to insure proper fit of adjacent atom sheets. It has been demonstrated that the magnitudes

of these parameters may be predicted accurately from basic crystal data and plane geometry. Other structural properties such as apparent anisotropic thermal motion may be correlated to substitutional disorder within atom sheets, while polytypism and twinning in micas is most conveniently discussed in terms of stacking variations between these sheets. Thus, simple geometrical models may be used to understand more fully the crystal chemistry of these and other layer silicates.

### Acknowledgments

The authors gratefully acknowledge the contributions of Professor J. B. Thompson of Harvard University and Dr. D. R. Wones of the United States Geological Survey. Their stimulating discussions and careful review of the manuscript have greatly improved the quality of this work. Special thanks are also due to Professor Roger Burns of the Massachusetts Institute of Technology, and to Dr. Jun Ito and Mr. Stephen Roberts of Harvard University, for aid in Mössbauer, wet chemical, and microprobe analysis, respectively. We are indebted to Professor Clifford Frondel of the Harvard Museum and Dr. Fred Barker of the United States Geological Survey for providing specimens for study. Finally, we wish to thank Dr. J. R. Smyth, Dr. Y. Ohashi, and Mr. T. L. Grove for their aid and advice in both laboratory and computational aspects of this study.

Research on the crystal chemistry of silicates was supported by National Science Foundation Grant GA-12852.

### References

- BARKER, FRED, D. R. WONES, W. N. SHARP, AND G. A. DESBOROUGH (1972) Some aspects of the chemistry, mineralogy, petrology, and genesis of the Pikes Peak batholith, Colorado. *Geol. Soc. Amer. Abstr. Programs*, **4**, 444.
- BRAGG, W. L., G. F. CLARINGBULL, AND W. H. TAYLOR (1965) *The Crystal Structures of Minerals*. Cornell University Press, Ithaca, N.Y., 409 pp.
- BURNHAM, C. W. (1962) Lattice constant refinement. *Carnegie Inst. Washington Year Book*, **61**, 132-135.
- (1965) Temperature parameters of silicate crystal structures (abstr.). *Amer. Mineral.* **50**, 282.
- (1966) Computation of absorption correction and the significance of end-effect. *Amer. Mineral.* **51**, 159-167.
- , Y. OHASHI, S. S. HAFNER, AND D. VIRGO (1971) Cation distribution and atomic thermal vibrations in an iron-rich orthopyroxene. *Amer. Mineral.* **56**, 850-876.
- , AND E. W. RADOSLOVICH (1964) Crystal structures of coexisting muscovite and paragonite. *Carnegie Inst. Washington Year Book*, **63**, 232-236.
- DONNAY, G., J. D. H. DONNAY, AND H. TAKEDA (1964a) Trioctahedral one-layer micas. II. Prediction of the structure from composition and cell dimensions. *Acta Crystallogr.* **17**, 1374-1381.
- , N. MORIMOTO, H. TAKEDA, AND J. D. H. DONNAY (1964b) Trioctahedral one-layer micas. I. Crystal structure of a synthetic iron mica. *Acta Crystallogr.* **17**, 1369-1373.

- FINGER, L. (1969) Determination of cation distribution by least-squares refinement of single-crystal x-ray data. *Carnegie Inst. Washington Year Book*, **67**, 216–217.
- FOSTER, M. D. (1960) Interpretation of the composition of trioctahedral micas. *U. S. Geol. Surv. Prof. Pap.* **354-B**, 11–46.
- FRANZINI, M., AND SCHIAFFINO (1963) On the crystal structure of biotite. *Z. Kristallogr.* **119**, 297–309.
- GÜVEN, N. (1967) The crystal structure of  $2M_1$  phengite and  $2M_1$  muscovite. *Carnegie Inst. Washington Year Book*, **66**, 487–492.
- , AND C. W. BURNHAM (1967) The crystal structure of  $3T$  muscovite. *Z. Kristallogr.* **125**, 163–183.
- HAMILTON, W. C. (1959) On the isotropic temperature factor equivalent to a given anisotropic temperature factor. *Acta Crystallogr.* **12**, 609–610.
- HATCH, R. A., R. A. HUMPHREY, W. EITEL, AND J. E. COMEFORO (1957) Synthetic mica investigations. IX. Review of progress from 1947–1955. *U. S. Bur. Mines Rep. Invest.* **5337**.
- HAZEN, R. M., AND D. R. WONES (1972) The effect of cation substitutions on the physical properties of trioctahedral micas. *Amer. Mineral.* **57**, 103–125.
- HENDRICKS, S. B., AND M. JEFFERSON (1939) Polymorphism of the micas. *Amer. Mineral.* **24**, 729–771.
- International Tables for X-ray Crystallography* (1962) Vol. III. Kynoch Press, Birmingham, England.
- JACKSON, W. W., AND J. WEST (1930) The crystal structure of muscovite. *Z. Kristallogr.* **76**, 211–227.
- , AND ——— (1933) The crystal structure of muscovite. *Z. Kristallogr.* **85**, 160–164.
- MCCAULEY, J. W. (1968) *Crystal structures of the micas  $KMg_3AlSi_3O_{10}F_2$  and  $BaLiMg_2AlSi_3O_{10}F_2$* . Ph.D. Thesis, Pennsylvania State University.
- , R. E. NEWNHAM, AND G. V. GIBBS (1973) Crystal structure analysis of synthetic fluorophlogopite. *Amer. Mineral.* **58**, 249–254.
- MAUGUIN, M. CH. (1927) Étude du mica muscovite au moyens des rayons X. *C.R. Acad. Sci. Paris*, **185**, 288–291.
- (1928) Études des micas non fluores au moyens des rayons X. *C.R. Acad. Sci. Paris*, **186**, 879–881.
- PABST, A. (1955) Redescription of the single layer structure of the micas. *Amer. Mineral.* **40**, 967–974.
- PAULING, L. (1930) The structure of micas and related minerals. *Proc. Nat. Acad. Sci.* **16**, 123–129.
- RADOSLOVICH, E. W., AND K. NORRISH (1962) The cell dimensions and symmetry of layer lattice silicates. I. Some structural considerations. *Amer. Mineral.* **47**, 599–616.
- ROSS, M., H. TAKEDA, AND D. R. WONES (1966) Mica polytypes: systematic description and identification. *Science*, **151**, 191–193.
- SHANNON, R. D., AND C. T. PREWITT (1969) Effective ionic radii in oxides and fluorides. *Acta Crystallogr.* **B25**, 925–934.
- , AND ——— (1970) Revised values of effective ionic radii. *Acta Crystallogr.* **B26**, 1046–1048.
- SMITH, J. V., AND S. W. BAILEY (1963) Second review of Al–O and Si–O tetrahedral distances. *Acta Crystallogr.* **16**, 801–811.
- , AND H. S. YODER (1956) Experimental and theoretical studies of the mica polymorphs. *Mineral. Mag.* **31**, 209–235.
- STEINFINK, H. (1962) Crystal structure of a trioctahedral mica: phlogopite. *Amer. Mineral.* **47**, 886–896.
- TAKEDA, H., AND C. W. BURNHAM (1969) Fluor-polyolithionite: a lithium mica with nearly hexagonal ( $Si_3O_9$ ) ring. *Mineral. J.* **6**, 102–109.
- , AND J. D. H. DONNAY (1966) Trioctahedral one-layer micas. III. Crystal structure of a synthetic lithium fluor-mica. *Acta Crystallogr.* **20**, 638–646.
- TAKEUCHI, Y., AND R. SADANAGA (1959) The crystal structure of xanthophyllite. *Acta Crystallogr.* **12**, 945–946.
- , AND ——— (1966) The crystal structure of xanthophyllite revised. *Mineral. J.* **4**, 421–437.
- TEIPKIN, E. V., V. A. DRITS, AND V. A. ALEXANDROVA (1969) Crystal structure of iron biotite and construction of several structural models for trioctahedral micas. *Proc. Int. Clay Conf.*, Vol. **1**, Tokyo.
- WONES, D. R. (1963) Physical properties of synthetic biotites on the join phlogopite-annite. *Amer. Mineral.* **48**, 1300–1321.
- ZVYAGIN, B. B., AND K. S. MISHCHENKO (1962) Electronographic data on the structure of phlogopite-biotite. *Sov. Phys. Crystallogr.* **7**, 502–505.

Manuscript received, February 16, 1973; accepted for publication, May 25, 1973.